Chapter 4

Perovskites-Based Nanomaterials for Chemical Sensors

Morteza Enhessari and Ali Salehabadi

Additional information is available at the end of the chapter

http://dx.doi.org/10.5772/62559

Abstract

The perovskite structure is adopted by many compounds in solid-state chemistry. The sensitivity, selectivity, and stability of many perovskite nanomaterials have been devoted the most attention for chemical sensors. They are capable to sense the level of small molecules such as O_2, NO, and CO. This chapter provides a comprehensive overview of perovskite nanoscale materials that concentrate on chemical sensors. The perovskite structure, with two differently sized cations, is amenable to a variety of dopant additions. This flexibility allows for the control of transport and catalytic properties, which are important for improving sensor performance. We devote the most attention on the synthesis, structural information, and sensing mechanism. We will later elaborate on the development mechanism of chemical sensors based on perovskite nanomaterials. We conclude this chapter with the personal perspectives on the directions toward future works on a novelty of nanostructured chemical sensors.

Keywords: Perovskite, Nanomaterial, Chemical sensor, Gas sensing material, Semiconductor

1. Introduction

The 3D-metal monooxides such as MnO, FeO, CoO, and NiO are semiconductors with low electrical conductivities. In general, the as-mentioned metal oxides have such large band gaps that they are insulators. The structure with general formula ABX_3, containing 12-coordinate hole of BX_3 is occupied by a large A ion (A: Ni, Pb, Fe, Co, Zn, etc) are known as perovskites. The tetragonal structure of perovskites showing the local displacements leads to the variation in electric behavior of this material (**Figure 1**).

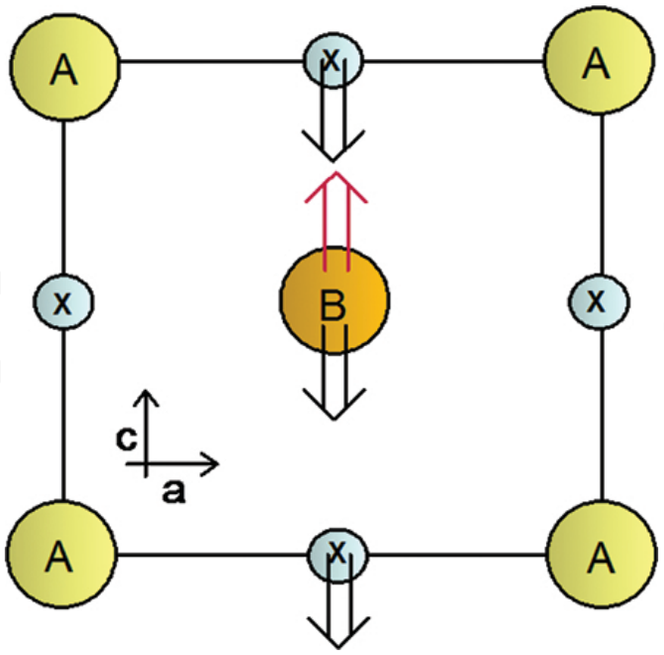

Figure 1. The local ion displacements of a tetragonal ABX_3 structure [1].

Many applications of perovskites (here ABO_3) are reported in electrodes of solid oxide fuel cells [2], metal–air batteries [3], gas sensors [4], and high-performance catalysts [5].

Metal-oxide semiconductors, such as semiconducting tin oxide (SnO_2), have been used as chemical sensors for a number of years. Applications include environmental monitoring, fire detection, and vehicle monitoring [4]. The fundamental sensing mechanism of these metal-oxide-based gas sensors relies upon the change in electrical conductivity due to the interaction between the gases in the environment and oxygen in the grain boundaries.

A chemical sensor is a device that transforms chemical information into an analytically useful signal. The chemical information may originate from a chemical reaction of the analyte or from a physical property of the investigated system. They have applications in different areas such as medicine, home safety, environmental pollution, and many others. Chemical sensors are classified according to the operating principle of the transducer (**Table 1**).

A variety of chemical methods have been reported for the synthesis of semiconducting materials including perovskites, spinels, or illminites which include ball-milling [6, 7], combustion synthesis [8–10], co-precipitation [11], sol–gel [12–15], radio frequency sputtering [16–19], solid-state reaction [20–22], and molten-salt method [23, 24].

In this chapter, we will review the routine reliable synthesis method, structural information, and gas sensing behavior of (mixed) metal-oxide semiconductors with tunable functionalities used in electrical devices for chemical sensors. Novel functional nanostructure semiconductors will be presented.

http://dx.doi.org/10.5772/62559

Type of chemical sensor	Source	Example
Oprical (optodes)	Optical phenomena	Absorbance, reflectance
		Luminescence
		Fluorescence
		Opto-thermal effect
		Light scattering
Electro chemical	Electrochemical process	Voltammetric sensors
		Potentiometric sensors
		Chemically sensitized field effect transistor potentiometric solid electrolyte gas sensors
Electrical	Electrical properties	Metal-oxide semiconductor
		Organic semiconductor
		Electrolytic conductivity
		Electric permittivity
Mass sensitive	Mass change at a specially modified surface	Piezoelectric devices
		Surface acoustic wave devices
Magnetic	Change of paramagnetic properties	Oxygen monitors
Thermometric	Heat effects of a specific chemical reaction or adsorption	Combustion reaction
		Enzymatic reaction
		Optothermal device
Radiation	Change of Physical properties	X-, p- or r-radiation
		Chemical composition

Table 1. Classification of chemical sensors

1.1. Semiconductors chemistry

Semiconductors are insulators at absolute zero. Above this temperature and below the melting point of the solid, the metal acts as a semiconductor. Semiconductors are generally classified on the basis of their composition and particle size. Procreation of semiconductors with typical band gaps (a few eV's corresponding to 100–200 kJ mol^{-1}) usually occurs between *p*-block metals and group 13/14 metalloids in combination with *chalcogenides* and *pnictides* [1].

Perovskites are an example of especial class of semiconductors (**Figure 2**). In this structure, the unit cell is not centrosymmetric and the crystal develops a permanent electric polarization as

a result of ion displacements (refer to **Figure 1**). Barium titanate, $BaTiO_3$, is one of the interesting examples of perovskite. This compound, at above 120°C, exhibits a cubic structure while a lower symmetry, that is, a tetragonal unit cell at room temperature due to ions displacement. Fe_2TiO_5 [25], $NiTiO_3$ [26, 27], $CoTiO_3$ [15, 28], $BaZrO_3$ [12], La_2CuO_4 [29], $LaMnO_3$ [5], $MnTiO_3$ [14], and $PbTiO_3$ [30] are some important examples of common perovskite oxide semiconductors.

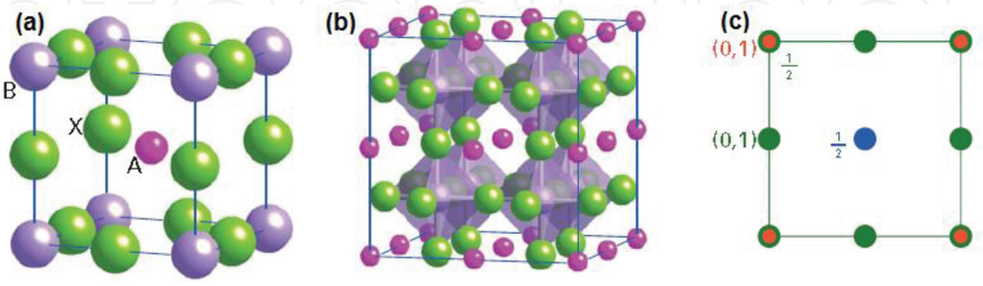

Figure 2. Schematic representation of (a) perovskite (ABX_3) structure, (b) emphasizes of octahedral sites, and (c) its respective projection [1].

1.2. Semiconducting Chemical Sensors

Chemical sensors are generally classified according to the shape of metal oxides to nanotubes, nanorods, nanobelts, and nanowires [16]. A nanotube sensors include metal-oxide tubes such as Co_3O_4 (superior gas sensing capabilities toward H_2), SnO_2 (gas sensor to ethanol), and TiO_2 (hydrogen sensor). Nanorod-based sensors are involved in metal oxides such as ZnO, MoO_3, and tungsten oxide nanosensors, polymer nanorods such as poly(3,4-ethylene-dioxythiophene)-nanosensor, and metal nanorods such as Au nanosensor. As for nanobelt-based sensors, the attentions have been devoted on metal oxides such as ZnO (Co and O_2 sensors), SnO_2 (NO_2 sensors), and V_2O_5 (stable ethanol sensor) nanosensors, especially on ZnO nanobelts sensors. Nanowire metal oxides such as In_2O_3, SnO_2, ZnO, and Ga_2O_3 are used in NO_2 sensor, O_2 and CO sensors, NH_3 sensor, and ethanol sensor, respectively.

Perovskites with a general formula of ABO_3, a typical band gap of 3–4 eV and good thermal stability, are interesting choices for gas sensing materials [6]. A suitable material for a chemical sensor particularly gas sensors must not only have an appropriate electronic structure but also a good affinity with the target reactant which satisfies a number of other requirements such as manufacturability, hydrothermal stability, poisoning resistance, and adaptability with existing technologies. A wide variety of techniques are capable of synthesizing perovskites (nano)- materials. Sol–gel, impregnation, and precipitation are some of the most promising ones from efficiency and scale-up perspectives.

Many researchers have reported the gas sensing devices for dangerous gases such as carbon oxides (CO, CO_2), nitrogen oxides (NO, NO_2), and sulfur dioxide (SO_2) released from high-temperature combustion processes. CH_4 is another potent greenhouse gas that leads to global warming [31–34].

http://dx.doi.org/10.5772/62559

The perovskite oxide generally used in oxygen sensors is $SrTiO_3$ [35]. The oxygen partial pressure dependence of the conductivity of undoped $SrTiO_3$ contains both n-type and p-type regimes.

Gas sensing properties of nanocrystalline perovskite, $LaFeO_3$ [36] and $BaTiO_3$ [37], were successfully involved in previous literatures. It is concluded that the sensor based on the $LaFeO_3$ powders has a considerable sensing response to carbon dioxide. On the other hand, the $BaTiO_3$ sensor has a good selectivity to LPG against CO_2, H_2, NH_3, C_2H_5OH, and Cl_2. The $BaTiO_3$ thin films exhibit rapid response recovery which is one of the main features of this sensor. The defect structure and conduction properties of $BaTiO_3$ are also similar to those of $SrTiO_3$. However, the conductivity of $BaTiO_3$ is higher than that of $SrTiO_3$ in the p-type regime.

Hydrogen-sensitive semiconductor $SrCe_{0.9}Yb_{0.1}O_3$ nanopowders with tunable sensing functionalities toward H_2 and H_2S were synthesized in our group [13]. We observed a noticeable gas sensing behavior of the perovskite at room temperatures with semi-spherical and porous structures of nanoparticles.

High sensitivity and selectivity of mixed potential sensor based on Pt/YSZ/$SmFeO_3$ for NO_2 gas are investigated by Giang et al. [38]. They concluded that the high sensing performances of the as-mentioned sensor to NO_2 could be related to high catalytic active of the sensing material, that is, $SmFeO_3$. The adsorption of exposed gases on the surface of $SmFeO_3$ has been considered the factor that affects on the performance of the sensor Pt/YSZ-8/$SmFeO_3$.

CO sensitive nanocrystalline $LaCoO_3$ and $La_{1-x}Ce_xCoO_3$ perovskite sensor were investigated by Dhivia et al. [6] and Ghasdi et al. [31]. They inferred that the oxygen mobility increased by increasing the surface area. Moreover, the maximum response ratio of CO exhibited a good correlation with the total amount of desorbed oxygen.

Hydrocarbon gas sensing of nanocrystalline perovskite oxides, $LnFeO_3$, shows a superior response to gas sensing characteristics containing methane, propane, and n-hexane. Moreover, the rare earth elements of the as-mentioned perovskite play an important role to gas sensitivities [39].

Nanostructured perovskite, $CdTiO_3$ films for methane sensing, is one of the recent studied examples of semiconductor for chemical sensors [40]. The gas sensing mechanism of $CdTiO_3$ sensor is of surface-controlled type. The variation in the resistance of sensing material caused by the adsorption and desorption of gas molecules such as O_2. The oxygen adsorption on the $CdTiO_3$ film surface depends on the temperature. At high temperatures, O_2 dissociates into atomic oxygen $O^-_{(ads)}$(Eq. 1)

$$\begin{aligned} &O_{2(\text{gas})} \leftrightarrow O_{2(\text{ads})} \\ &O_{2(\text{ads})} + e^- \rightarrow O^-_{2(\text{ads})} \\ &O^-_{2(\text{ads})} + e^- \rightarrow 2O^-_{(\text{ads})} \end{aligned} \tag{1}$$

The chemistry image, the classification of perovskites applicable as gas sensing materials, the fabrications, and the performance mechanism of gas sensors will be discussed in the following sections. It must be noted that in this chapter the perovskites classes are named based on "B" site in general formula of ABO_3, such as stanate ($BaSnO_3$), titanate, and niobate.

2. Classification of perovskites

As mentioned before, the typical chemical formula of the perovskite structure is ABO_3 and AB_2O_4, where A and B denote two different cations. The ilmenite structure has the same composition as the perovskite, that is, ABO_3; however, A and B in this structure are cations of approximately the same size that occupy an octahedral site.

Compound	Lattice parameter/× 10 nm		
	A	B	c
		Cubic structure	
$KTaO_3$	3.989		
$NaTaO_3$	3.929		
$NaNbO_3$	3.949		
$BaMnO_3$	4.040		
$BaZrO_3$	4.193		
$SrTiO_3$	3.904		
$KMnF_3$	4.189		
$KFeF_3$	4.121		
		Tetragonal structure	
$BiAlO_3$	7.61		7.94
$PbSnO_3$	7.86		8.13
$BaTiO_3$	3.994		4.038
$PdTiO_3$	3.899		4.153
$TlMnCl_3$	5.02		5.04
		$LaAlO_3$ type	
$LaAlO_3$	5.357	α=60° 06′	
$LaNiO_3$	5.461	α=60° 05′	
$BiFeO_3$	5.632	α=60° 06′	
$KNbO_3$	4.016	α=60° 06′	
		$GdFeO_3$ type	
$GdFeO_3$	5.346	5.616	7.668
$YFeO_3$	5.283	5.592	7.603
$NdGaO_3$	5.426	5.502	7.706
$CaTiO_3$	5.381	5.443	7.645
$NaMgF_3$	5.363	5.503	7.676

Table 2. Typical perovskite compound [41]

http://dx.doi.org/10.5772/62559

Various combinations of charged cations in the A and B sites of perovskite compounds such as 1 + 5 and 2 + 4 have been reported. However, a complex combinations are also investigated, such as $M(B'_{1/2}B''_{1/2})O_3$, where M can be Pb or La, B′ can be Sc, Fe, Ni, or Mg and B″: Nb, Ta, Ru(IV), or Ir(IV). Typical perovskite compounds with various lattice structures are listed in **Table 2**.

In **Table 3**, the as-reported elements that can be incorporated within the perovskite structure are listed (Self-test: to be completed by the readers). It is obvious that almost all elements except noble gases can be occupied either A or B lattice structure in the perovskite lattice. The crystal structure of perovskites is dependent on the size and the nature of the A and B atoms. Simplifying the possible lattice interaction between elements forms a perovskite structure for gas sensing materials.

B/A	Na	K	Rb	Ca	Sr	Ba	Y	La	Hf	Ag	Cd	Ln	Tl	Pb	Ce	Th	Pr	Nd	Sm	Eu	Gd	Tb	Dy	Ho	Er	Tm	Yb	Lu	Th
Li																													
Mg																													
Sc																													
Ti				✓	✓			✓						✓															
Zr														✓															
V																													
Nb	✓	✓				✓																							
Ta		✓																											
Cr				✓			✓	✓																					
Mo																													
W																													
Mn				✓	✓		✓	✓																					
Tc																													
Re																													
Fe		✓		✓	✓	✓		✓*				✓			✓				✓										
Ru																													
Os																													
Co						✓	✓	✓							✓														
Ni						✓		✓																					
Pd					✓																								
Pt																													
Cu		✓																											
Zn																													
Al																													
Ga																													
In																													
Ge																													
Sn				✓		✓																							
U																													
Np																													
Pu																													

"✓" Represents the available, as-synthesized gas sensing perovskites; "*" corresponds to $LaFeO_3$ [42].

Table 3. (Self-test) elements that can occupy perovskite structure (ABO_3, AB_2O_4)

Another class of perovskites forms by the replacement of B-site elements with a dopant. The as-mentioned structure with general formula $A_3MB_2O_9$ is called as superstructure perovskites. In fact, large differences in ionic radii lead to the formation of this huge structure. Here, M can be Fe, Co, Ni, Zn, or Ca like $Ba_3SrTa_2O_9$. Moreover, a new class of superstructure perovskite is invented where the ordering of cation vacancies located on A sites: for example, MNb_3O_9 (M-La, Ce, Pr, Nb) and MTa_3O_9 (M-La, Ce, Pr, Nd, Sm, Gd, Dy, Ho, Y, Er).

Typical polymorphs of the perovskite structure are brownmillerite ($A_2B_2O_5$). This is oxygen deficient type of perovskite, the oxygen vacancy is ordered [41, 43]. In this structure, as the content of oxygen drops, the phase changes from the cubic perovskite to tetragonal, to orthorhombic, and finally to the brownmillerite structure. These phases are in fact a repeating sequence of octahedral and tetrahedral layers [44]. In the typical example of a non-stoichiometric ternary oxide such as $SrFeO_{2.5+x}$ ($0 < x < 0.5$), there is a series of phases that is derived from the perovskite structure. Stepwise dropping of the oxygen content, the phase changes from the cubic ($x = 0.5$) to tetragonal ($x = 0.35$), to orthorhombic ($x = 0.25$), and to the brownmillerite structure ($x = 0$) [43, 44]. The as-mentioned phenomenon can be observed clearly in the reaction isotherm profiles (**Figure 3**). In the regions where two phases co-exist, the x-value increases greatly for the small increase in oxygen pressure.

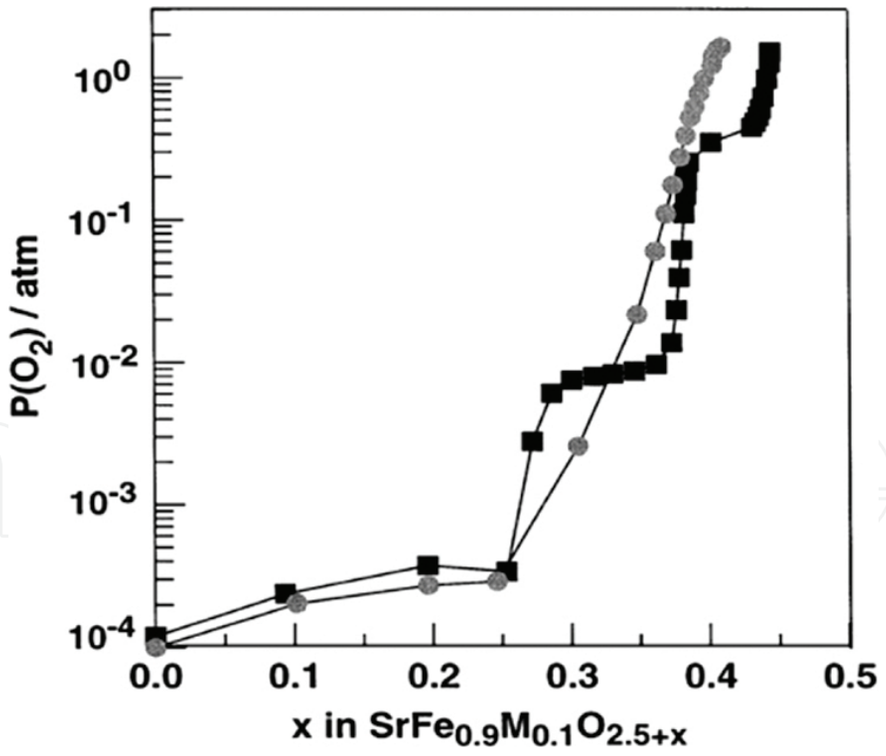

Figure 3. Reaction isotherm of $SrFeO_{2.5+x}$ in a substituted $SrFe_{0.9}Cu_{0.1}O_{2.5}$ [44].

Ruddelsden–Popper compounds are a group of perovskite with the general formula $(ABO_3)_nAO$ (**Figure 4**). Some examples of this structure are $Sr_3Ti_2O_7$ and $Sr_4Ti_3O_{10}$.

http://dx.doi.org/10.5772/62559

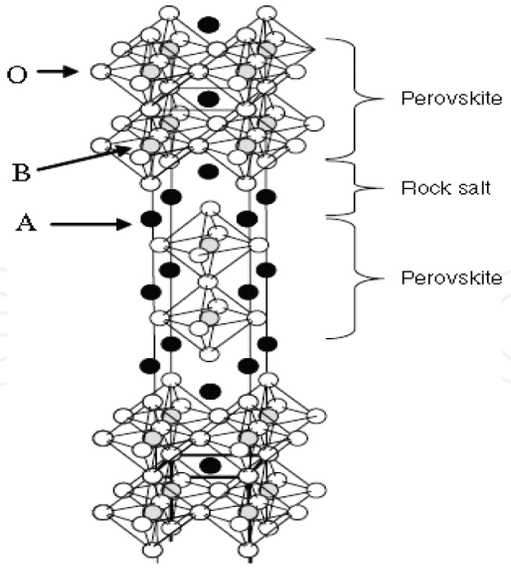

Figure 4. Ruddelsden–popper structure [41].

3. Sensing materials and mechanism

Sensor technology has widely distributed as a basic enabling technology in many instances. Many applications of sensing devices particularly in intelligent manufacturing processing have been reported ranging from assessing the integrity of aircraft to monitoring the environment for hazardous chemicals [45, 46]. The oxygen deficient crystal structure in semiconducting oxide materials is responsible for the change in resistance an oxide sensor [1]. This is due to the adsorbed surface species [41]. The reducing gas develops a shrink charge region which allows better charge movement.

A chemical/gas sensor provides an electrical/optical output in response to chemical and physical interactions with chemicals/gases. In particular, the gas sensors have been used for various industrial and/or safety applications and chemical such as a) determination of gas leakage [41, 47–49], novel LPG sensitive materials working in the entire range of least explosive limit (LEL) to upper explosive limit (UEL) [30–32]. Nanostructured perovskite materials can improve the sensing properties of the sensor due to high surface-to-volume ratio characteristics. Knowledge of nanoscale perovskite sensing materials have been achieved a great attraction to serve as a novel gas sensing materials at the lower working temperatures.

How does a sensing materials work? Band theory is a principle of chemical sensors technology which postulates that when atoms or molecules are aggregated in the solid state, the outer atomic orbitals are split into bonding and antibonding orbitals and mix to form two series of closely spaced energy levels. In general, in a gas sensor, the gas species react with metal-oxide particle surfaces thereby trapping electrons (**Figure 5**). This is the process of chemisorptions. A resistance layer from an electron-depleted space (cloud) charge on the n-type (the majority of charge carriers are electrons) particle surface or conducting layer from accumulated holes on the p-type (the positive holes being the majority of charge carriers) particle [50]. Continued

reaction between gas molecules and chemisorbed oxygen causes electrons to release from oxygen back to oxide. The current changes the electrical conductivity in the space charge layer. The conductivity increases in the case of n-type oxides, as a greater charge carrier (electron) concentration, and decreases in p-type oxides, as electrons recombine with holes. Time-by-time changing of conductivity in the space charge layer varies the overall electrical resistance of the oxide. Hence, the space (cloud) charge surrounding the bulk material directly influenced the sensitivity, that is, thicker the space charge layer higher the sensitivity. The change of sensor resistance depends on a type of metal-oxide semiconductors, here perovskites. The changes in sensor resistance upon exposure to the target gas/reducing gas in the cases of n-type and p-type perovskite sensors are reported by Choopon et al. [51] as illustrated in **Figure 6**.

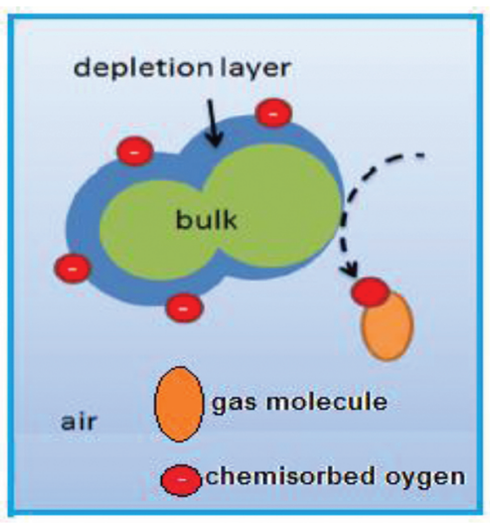

Figure 5. Mechanism of gas sensing [50].

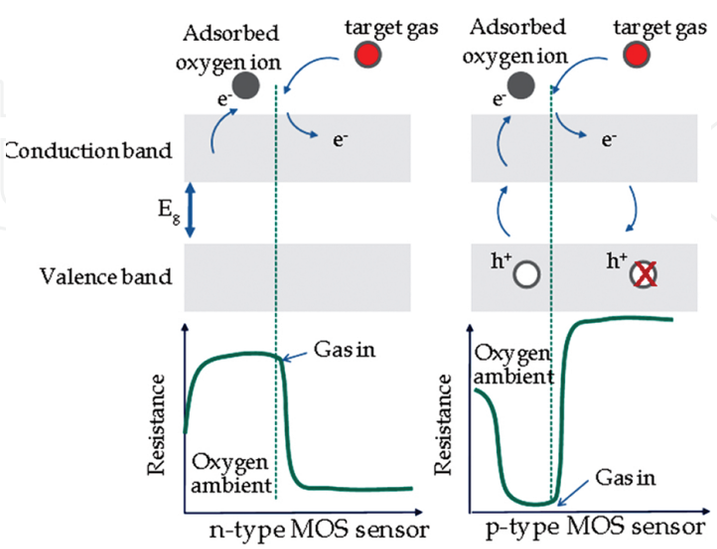

Figure 6. Change of sensor resistance upon exposure to the target gas [51].

4. Application of perovskite nanomaterials in gas sensor

Variety of component and high chemical stability are two important characteristic of perovskite nanomaterials applicable for catalysts in various reactions. It is impractical to consider the classification of perovskites without their applications in sensing devices. The advent of high-performance solid-state gas sensors has motivated several scientists in searching the new perovskite materials and investigating their gas sensing properties. In general, the perovskites are either oxidation catalysts or oxygen-activated catalysts as an alternative to catalyst containing precious metals, or a model for active sites. The stability of the perovskite structure allows the invention of new compounds with an unusual valence state of elements or a high extent of oxygen deficiency [41]. In **Table 4**, we summarize the as-reported perovskite nanomaterials in sensing device. We mentioned that the high catalytic activity of perovskite oxides is based on the high surface activity to oxygen reduction ratio or large number of oxygen vacancies in the particular structure. Among the various catalytic reactions studied, automobile exhaust gas, various pollutant gases such as H_2S, and NH_3, NO_x decomposition reaction gas, hydrogen gas, methanol, and LP gas attract particular attention. The perovskite materials can be used as a thin film (nanocomposites) or nanopowders.

Sensing materials	NO_x	CH_4	NH_3	LPG	C_2H_5OH	Acetone	Refs.
Perovskite							
Titanate		$Sr(Ti_{0.65}Fe_{0.35})O_3$, $Pb(Zr_{0.2}Ti_{0.8})O_3$	$BaTiO_3$, $CdTiO_3$, $Na_2Ti_3O_7$		$Li_{0.35}La_{0.55}TiO_3$		[52–57]
Ferrite	$Cu_xFe_{3-x}O_4$, $Mg_{0.5}Zn_{0.5}Fe_2O_4$	$SrTi_{0.6}Fe_{0.4}O_{3-\delta}$ $BaFeO_3$	$La_{0.8}Sr_{0.2}Fe_{1-x}Cu_xO_3$, $Cu_{0.5}Zn_{0.5}W_{0.3}Fe_{1.7}O_4$	$Co_{1-x}Ni_xFe_2O_4$, $Mg_{0.5}Zn_{0.5}Fe_2O_4$		$NiFe_2O_4$	[17, 58–62]
Cobaltite		$Bi_{10}Co_{16}O_{38}$, $Ln_{1-x}Sr_xCoO_3$		$NdCoO_3$, $Nd_{0.8}Sr_{0.2}CoO_3$	$Bi_{12}(Bi_{0.55}Co_{0.45})O_{19.6}$ $LnBaCo_2O_{5+\delta}$, $Bi_{10}Co_{16}O_{38}$ $Ba_{0.5}Sr_{0.5}Co_{0.8}Fe_{0.2}O_{3-\delta}$		[63–69]
Cobaltate				$YCoO_3$, $LaCoO_3$ $La_{1-x}Ce_xCoO_3$ $NdCoO_3$			[6, 35, 60, 65–68]
Mangenate		$La_{0.8}Sr_{0.2}Al_{0.9}Mn_{0.1}O_3$, $Ln_{1-x}Ca(Sr)_xMnO_3$					[67, 70]
Cerate	$SrCe_{0.95}Yb_{0.05}O_{3-\alpha}$, $SrCeO_3$, $SrCe_{0.95}Tb_{0.05}O_{3-\delta}$		$BaCe_{0.90}Gd_{0.1}O_{3-\delta}$				[9, 71–73]
Niobate	$FeNbO_4$		$BaNbO_3$			$FeNbO_4$	[74, 75]
Nickelate				$LaNi0_3$			[76]
Stanate	$BaSnO_3$, Zn_2SnO_4, $ZnSnO_3$		$Ba_{1-x}Ni_xSnO_3$ $Ba_{1-x}La_xSnO_3$, $ZnSnO_3$	$BaSnO_3$			[77–83]
Zirconate	$PbZrO_3$		$CaZrO_3$				[20, 48, 84]
Chromate			$MgCr_2O_4$				[85, 86]
Molybdate	Bi_2MoO_6	$Bi_3FeMo_2O_{12}$	$ZnMoO_4$ $Bi_3FeO_4(MoO_4)_2$ $NiMoO_4$, $CuMoO_4$, $PbMoO_4$	$Bi_3FeMo_2O_{12}$			[87–89]
Tungstate	Sn_xWO_{3+x}		$ZnWO_4$, $MnWO_4$	$CoWO_4$, Sn_xWO_{3+x}, $SnW0_4$			[90–96]

Sensing materials	NO_x	CH_4	NH_3	LPG	C_2H_5OH	Acetone	Refs.
Perovskite							
Sensing materials	NO_x	CH_4	NH_3	LPG	C_2H_5OH	Acetone	Refs.
Perovskite							
Titanate				$ZnTiO_3$	$CoTiO_3$, $Cr_{1.7}Ti_{0.3}O_3$, Zn_2TiO_4,		[97–100]
Ferrite	$LaFeO_3$, $Co_{1-x}Mn_xFe_2O_4$, $CoFe_2O_4$	$Mg_{0.5}Zn_{0.5}Fe_2O_4$	$Ni_xZn_{1-x}Fe_2O_4$	$CuFe_2O_4$, $Ni_{1-x}Co_xFe_2O_4$	$Co_{1-x}Ni_xFe_2O_4$, $ZnFe_2O_4$, $Ni_xZn_{1-x}Fe_2O_4$, $GaFeO_3Ni_{1-x}Co_xFe_2O_4$ $Ni_{1-x}Co_xFe_2O_4$	$CoFe_2O_4$, $NiFe_2O_4$,	[11, 23, 47, 95, 96, 98–101]
Cobaltate	$YCoO_3$	$YCoO_3$					
Mangenate	$LaMnO_{3+\delta}$, $La_{0.6}Ca_{0.4}Mn_{1-x}Ni_xO_3$,						[42, 102]
Niobate		$LiNbO_3$	$CrNbO_4$, $InNbO_4$	$InNbO_4$, $FeNbO_4$	$AlNbO_4$, $CrNbO_4$, $InNbO_4$		[70, 97, 102–107]
Nickelate	$LaNi0_3$						[76]
Stanate	Zn_2SnO_4	Zn_2SnO_4	$CaSnO_3$, $ZnSnO_3$	Zn_2SnO_4, $ZnSnO_3$	$CaSnO_3$, Zn_2SnO_4,		[72–74, 108, 109]
Chromate					$LaCr_{1-x}Ti_xO_3$		[8]
Molybdate			Bi_2MoO_6, $NiMoO_4$		$Bi_3FeMo_2O_{12}$		[110, 111]
Tungstate	$CuWO_4$, $SnW0_4$, $MgWO_4$, $ZnWO_4$, $BaWO_4$		$CoWO_4$				[87–89, 110, 112]

Table 4. Gas sensing perovskite oxides

From **Table 4**, it is obvious that the various combinations of elements are used to produce the perovskite nanomaterials for the as-mentioned sensing devices. Among them, the humidity, LPG, ethanol, and pollution gases have been achieved a great attention.

Humidity measurement is one of the most significant issues in various areas of applications such as instrumentation, automated systems, agriculture, climatology, and GIS. Molybdate- , stanate- , and titanate-based perovskites are three powerful groups of materials used in this criterion. When perovskite oxides are exposed to moisture, interaction occurs in three stages: (a) a few water vapor molecules are chemisorbed at the neck of the crystalline grains on activated sites of the surface and form hydroxyl groups. As a result of this interaction, the hydroxyl group of each water molecule is adsorbed on metal cations and possesses high charge carrier density and strong electrostatic fields, and producing mobile protons. The protons migrate on the surface and react with the neighbor surface oxygen to form a second hydroxyl group. The chemisorbed layer is the first formed layer. (b) After chemical completion of the first layer, subsequent water vapor layers are physisorbed on the first-formed hydroxyl layer. After forming the first physisorbed layer, another water molecule adsorbs via double hydrogen bonding to two neighboring hydroxyl groups. This is continued to form multilayer. (c) By forming the more layers, a large amount of water molecules is physisorbed and bonded water vapor molecules become mobile and form continuous dipoles and electrolyte layers between the electrodes to generate dielectric constant and bulk conductivity. **Figure 7** shows the layer by layer adsorption of humidity on the ceramic intelligent surface.

http://dx.doi.org/10.5772/62559

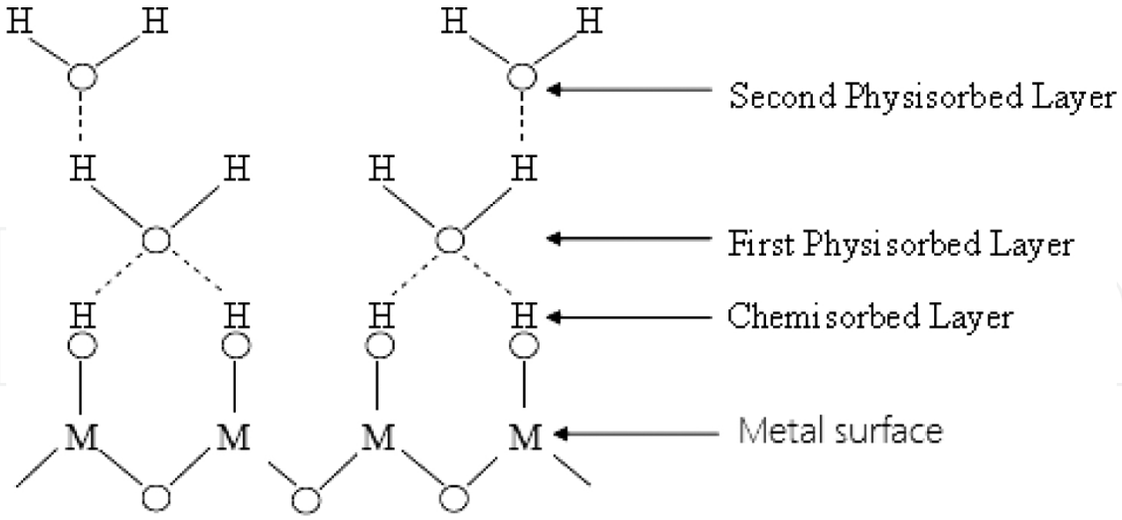

Figure 7. Mechanism of humidity sensing [113].

Ferrite and cobaltate/cobaltite are two main groups of materials used as active sites in CO sensing device. The mechanism of CO sensors is based on an anionic adsorption and the lattice oxygen atoms activities in the surface of perovskites ceramic. Here, the oxygen atoms are adsorbed and react with the available CO gases to form CO_2 and generate a free electron [114] of following types (Eq. 2):

$$\begin{aligned}
&O_{ads.} + CO \Rightarrow CO_2 + e \\
&CO_g \Rightarrow CO_{aq.} \Rightarrow CO^{+}_{ads.} + e \\
&CO_{ads.} + O_2 \Rightarrow CO_2 + e \\
&CO_g + O^{x}_{o} \Rightarrow CO_2 + e + V^{x}_{o} \\
&CO + 1/2\, O_2 + V^{x}_{o} + e \Rightarrow CO_2 + O^{x}_{o}
\end{aligned} \tag{2}$$

A possible mechanism of oxidation of CO by lattice oxygen ions on the surface of La-doped $BaTiO_3$ is shown in **Figure 8**.

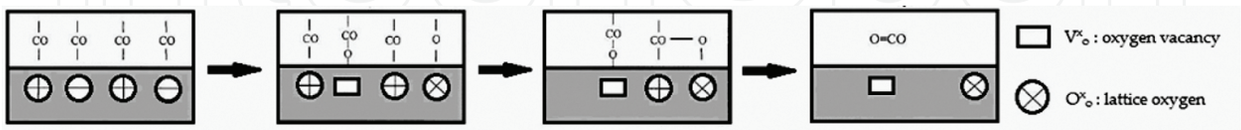

Figure 8. Schematic representation of CO absorption.

LPG (LPG is a mixture of hydrocarbons like n-propane and n-butane), ethanol, and NH_3 sensors are another classes of perovskite-based sensing devices with a variety of applications. The sensing mechanism follows almost the same mechanism. When the perovskite sensor is exposed to air, O_2 adsorbs on the surface substrate and trap electrons from the conduction

band of perovskites. This occurs due to the electronegativity of oxygen atom, negative-charged chemisorbed oxygen species, that is, O^{2-} and O^{-}. As a result, the number of holes increased, the resistance decreased, and the concentration of available carrier achieves a higher value. By exposing the sensing materials to reducing gases, the gas molecules first reacted with the adsorbed oxygen, the carrier (holes) density depressed (due to electron donating nature of gases), and finally increasing the resistance. The reaction mechanisms of LPG (Eq. 3), ethanol (Eq. 4), and NH_3 (Eq. 5) [115] are the following:

$$C_pH_{2p+2} + (3p+1)O^-_{(ads)} \rightarrow pCO_2 + (p+1)H_2O_{(g)} + (3p+1)e^- \quad (3)$$

$$C_2H_5OH + 6O^{n-}_{(ads)} \rightarrow 2CO_2 + 3H_2O + 6ne^- \quad (4)$$

$$2NH_3 + 3O^-_{(ads)} \rightarrow N_2 + 3H_2O + 3e^- \quad (5)$$

An example is $LaCo_xFe_{1-x}O_3$ nanoparticles which used to investigate the ethanol sensing properties [116]. A careful consideration on the response curves indicates that the $LaCo_{0.1}Fe_{0.9}O_3$ nanoparticles are very promising materials for fabricating ethanol sensors (**Figure 9**).

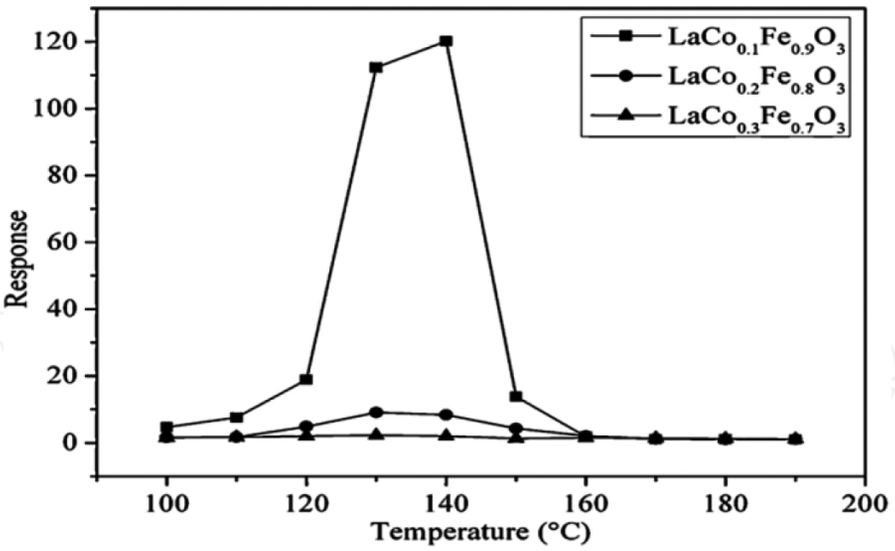

Figure 9. Responses of $LaFeO_3$, $LaCo_{0.1}Fe_{0.9}O_3$, $LaCo_{0.2}Fe_{0.8}O_3$, and $LaCo_{0.3}Fe_{0.7}O_3$ nanoparticles to 500 ppm ethanol [116].

Miscellaneous applications of perovskites in solid-state sensors such as infrared, electro-optic, heat, magnetic field, and liquid-state sensors especially in health-care products such as glucose and cholesterol are reported (**Table 5**). The form of the substrate is thick film including a

http://dx.doi.org/10.5772/62559

nanocomposite of perovskites and a polymer. Typical example of this class is $La_{0.67}Sr_{0.33}MnO_3$ (LSMO). A 400 nm thick LSMO films grow on the lucalox (polycrystalline Al_2O_3 + Mg) substrates *via* vapor deposition technique. Mechanism of such sensors is based on the change of the film resistivity depending on the applied magnetic field magnitude [119]. Initial resistance and the sensitivity to magnetic field are two important factors depend on ambient temperature. This is a drawback for magnetic field measurements because a temperature compensation mechanism is required. **Figure 10** shows a typical magnetic field LSMO sensor. Twisted wires solder to the parts of the electrodes above the substrate (uncovered). Some samples were covered with the polyethylene hot-melt adhesive.

Sensing materials	**Infrared**	**Magnetic field**	**Heat**	**Electro-optic**	**Glucose**	**H_2O_2**	**Cholesterol**	**NADH**	**Acetone**	**Refs.**
Perovskite										
Titanate		$Ba_{0.25}Sr_{0.75}TiO_3$								[117]
Ferrite					$LaTiO_3$, $ZnFe_2O_4$, $CuFe_2O_4$	$CoFe_2O_4$	$NiFe_2O_4$	$CoFe_2O_4$	$CoFe_2O_4$, $NiFe_2O_4$, $Ni_{1-x}Co_xFe_2O_4$	[47, 98–100, 118–121]
Mangenate	$Ni_xMn_{3-x}O_4$	$La_{0.67}Sr_{0.33}MnO_3$, La0 $_{.67}Ba_{0.33}O_3$ LaSrMnO, $La_{2/3}Sr_{1/3}MnO_3$, $La_{0.60}Pb_{0.40}MnO_3$								[119, 122–126]
Niobate			$LiNbO_3$	$KTa_{1-x}NbxO_3$						[45, 127]
Zirconate	$Pb(Zr_{52}Ti_4S)O_3$									[18, 128]

Table 5. Miscellaneous perovskites sensors

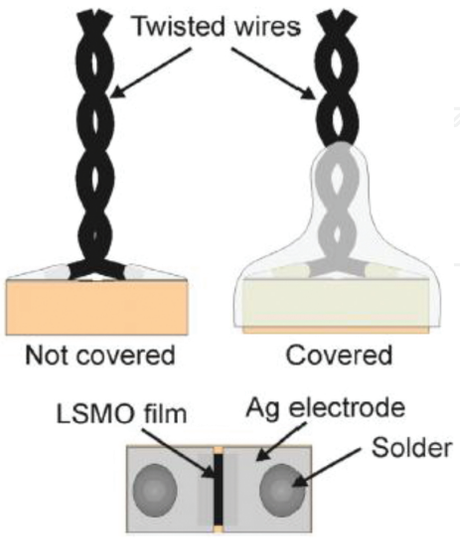

Figure 10. Covered and uncovered LSMO sensor (top and cross-section view) [119].

High selectivity, good sensitivity, fast, and reversible response are the main advantages of enzymatic glucose sensors (EGS) [129]. However, some deficiencies prevented wide range applications of EG sensors like the lack of mechanical and thermal stability and also environmental concerns. Development of glucose sensors without using enzymes based on magnetic nanoparticles can play a significant role. The nanoperovskites can be a good candidate due to the high surface area, high catalytic efficiency, superior mass transport, and strong adsorption ability [120]. Here, an electrode is covered/modified by intelligence perovskite nanomaterials or polymer-perovskite nanocomposite to enhance the sensing properties. In a typical example, polypyrrole is used as shell in polypyrrole–$ZnFe_2O_4$ magnetic nanocomposites to induce a strict barrier and reduce the magnetic coupling effect between nanoparticles (**Figure 11**). Electro-oxidation mechanism of glucose on $ZnFe_2O_4$/PPy core shell electrode is also shown [121].

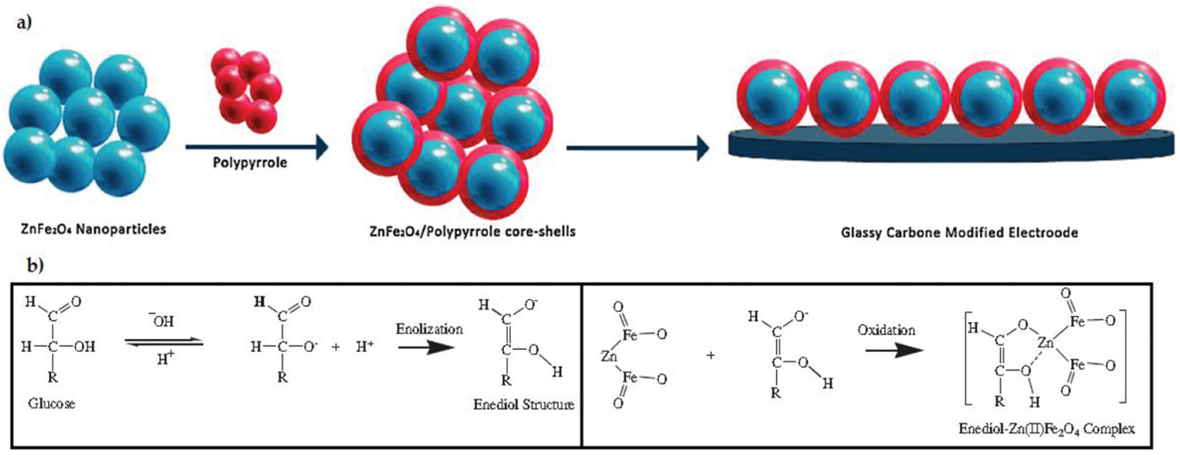

Figure 11 The illustration of (a) preparation process of modified electrode and (b) electro-oxidation mechanism of glucose on $ZnFe_2O_4$/PPy core-shell–glassy carbone modified electrode [121].

5. Fabrication of gas sensor

Various fabrication techniques have been developed in the production of metal-oxide semiconductor sensors. Purity, porosity, reliability, reproducibility, and expense are the most important factors in selecting the production technique [130]. The mechanism of gas sensors are discussed in previous sections. Thick film and thin film technologies have been popular techniques to minify various types of the sensors unifying in monolithic hybrid circuits. In the general definitions, thick film depositions are a process of surface modification by applying a thick coating on a substrate. The manufacture of such devices is multilayer coating film involving deposition of several layers deposition of conductor, resistor, and dielectric layers on the insulating substrate. Thin film technology is a process of deposition of required materials by applying a very thin coating layer often just a few nanometers thickness. Screen printing of ceramic powders, chemical vapor deposition (CVD), sol–gel techniques, spray pyrolysis, physical vapor deposition (PVD), and drop coating [130] are the main techniques for production of metal-oxide films for gas sensors.

http://dx.doi.org/10.5772/62559

5.1. Screen printing

Spiral shape sensing device (screen printing) is one of the simplest sensors in most of the as-reported research articles [13]. Intelligent ink pushes through a porous layer, and it contains the material to be deposited on the substrate. After complete deposition, the print is heated to remove the vehicle, leaving perovskites on the specific target area. **Figure 12** indicates a unit of gas sensor containing metal oxide fabricated by screen printing.

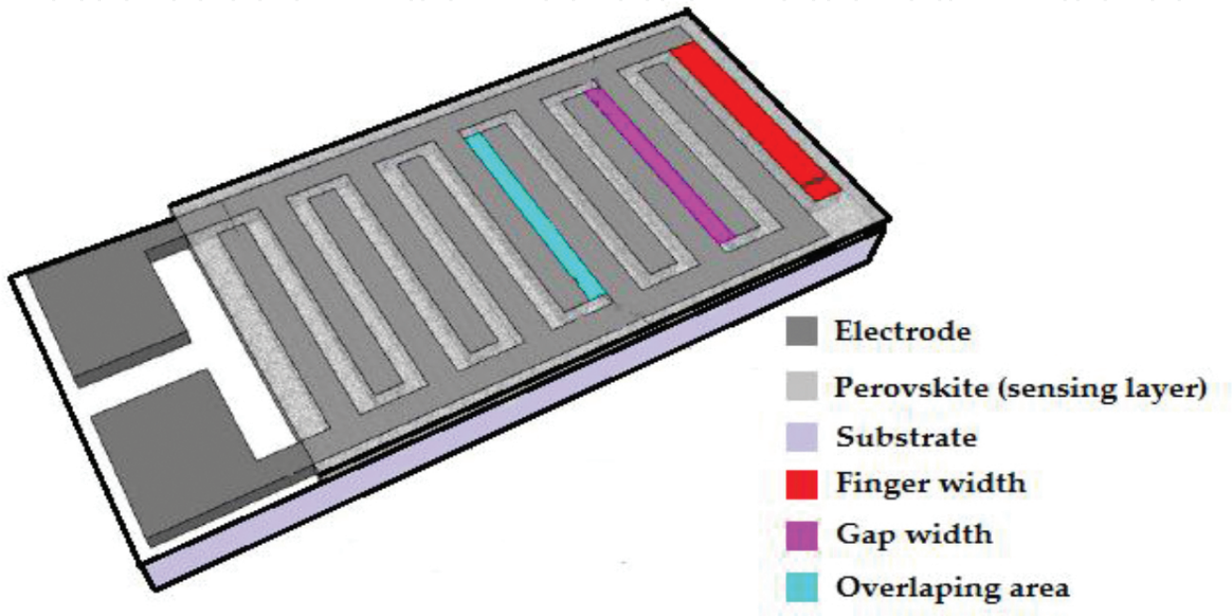

Figure 12. Unit of gas sensor fabricated by screen printing [113].

5.2. Chemical vapor deposition

A heated substrate is exposed to a precursor or controlled mixture of precursors in the vapor phase. The vapors finally interact on the substrate to form a film of the intelligent material. **Figure 13** demonstrates a gas sensors fabricated by CVD.

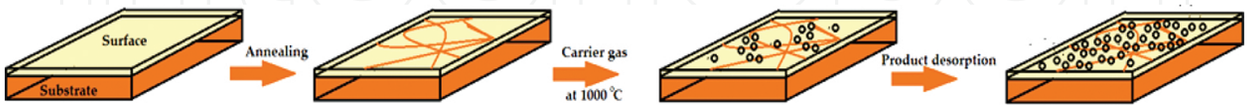

Figure 13. Gas sensor fabricated by chemical vapor deposition process.

5.3. Sol–gel

A film formation by sol–gel involves the formation of colloidal suspension of solid particles and cross-linking between particles, followed by evaporation, and finally heating the film to form a dense surface on the substrate (**Figure 14**).

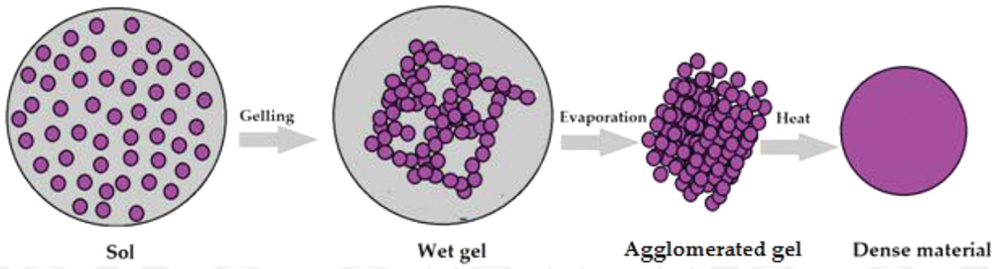

Figure 14. Gas sensing film fabricated via a sol–gel technique.

5.4. Spray pyrolysis

The reactants are sprayed on to the target substrate and then react on the surface by continuous heating to form film (**Figure 15**).

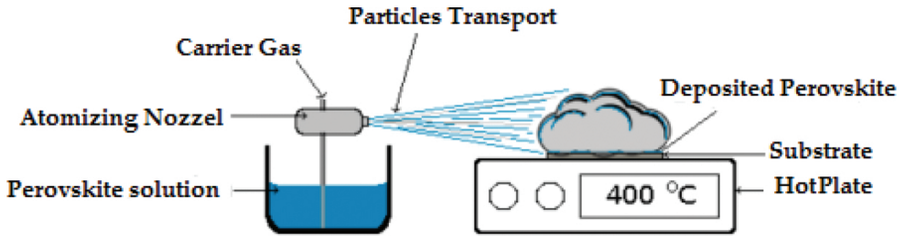

Figure 15. Schematic representation of spray pyrolysis [131].

5.5. Physical vapor deposition

The starting materials are transferred into the gas phase by evaporation/sputtering. A reactive gas reacts with the metal vapor, to form a compound, which further deposited on the substrate (**Figure 16**).

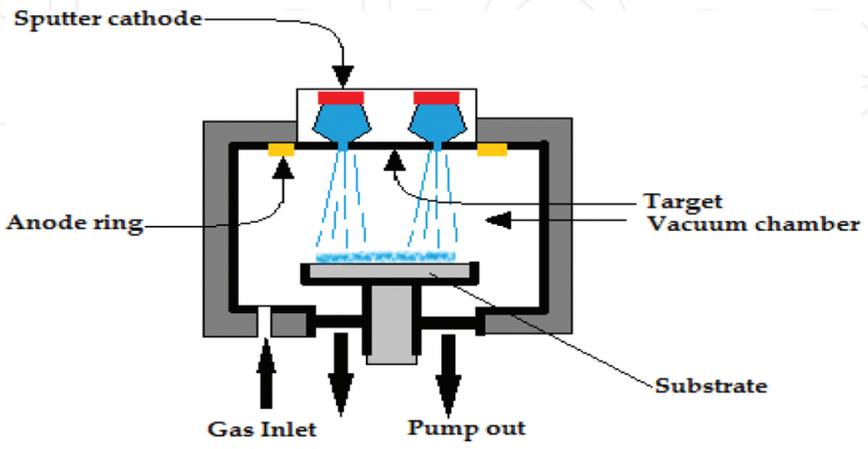

Figure 16. Unit of physical vapor deposition.

http://dx.doi.org/10.5772/62559

5.6. Drop coating

Drop coating is a process by where a paste is made of the desired perovskite powder and a solvent; the mixture is then deposited onto a substrate using an appropriate apparatus followed by the evaporation to form a film (**Figure 17**).

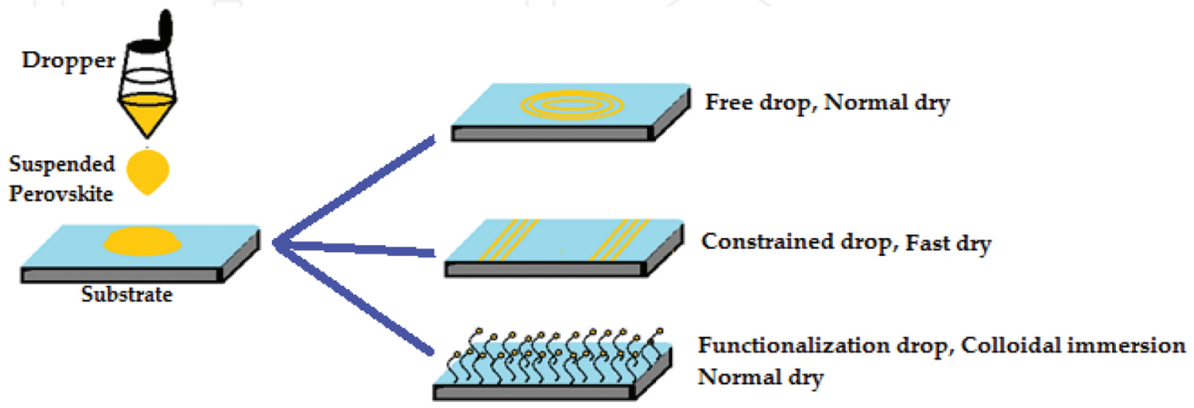

Figure 17. Drop coating sensor fabrication.

How does a real gas-sensor response to the analyte? The gas-sensor performance measures from the V_{out} of R_L that cascades R_s (the resistance of gas sensor). The resistance of gas sensor (R_s) and the sensor response (S) obtain from the (Eqs. 6 and 7), respectively;

$$R_S = R_L \left(V_c - V_{out}\right) / V_{out.} \tag{6}$$

$$S = R_a / R_g \tag{7}$$

where R_a is the resistance in air and R_g is the resistance in the air mixed with detected gases. The response time is the time required for the conductance to reach 90% of the equilibrium value after a test gas injection, and the recovery time was the time necessary for a sensor to attain a conductance 10% above its original value in air (**Figure 18**).

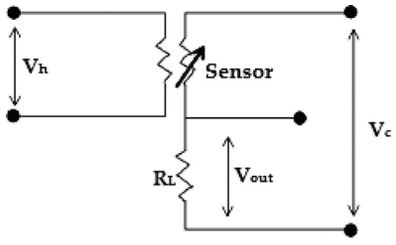

Figure 18. Electrical circuit diagram of a gas sensor [132].

For instance, $YCoO_3$-based sensors (p-type semiconductor) were tested at temperature range of 100–380°C. The obtained response to the gas (here NO_2) versus time can be given by the contribution of two different reactions: (a) oxidation and (b) reducing of the surface (**Figure 19**). The former is faster and favored at low temperature, and the latter is slower and favored at higher temperatures [133].

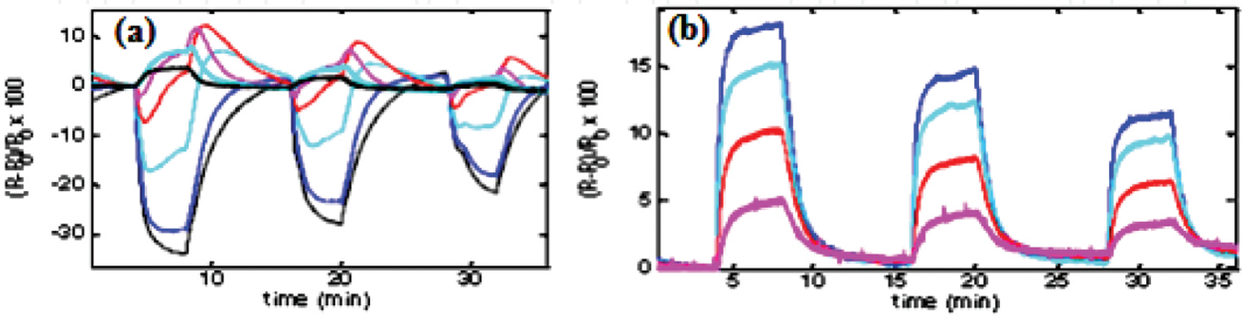

Figure 19. Typical response to (a) NO_2 and (b) CO at various temperature [133].

Artificial olfactory systems (AOS) based on metal-oxides chemiresistors is one of the devices which practically used for sensing the air pollutions. $YCoO_3$ sensors doped with various metals were selected for CO and NO_2 detection at different temperatures. At around 280°C, the sensor-doped Pd shows a satisfactory sensitivity with a large response speed to CO gas. The same electrode-doped Co was selected for NO_2 pollution sensing. The results clearly indicate that a good sensitivity and a fast response (response time, $T_{10–90\%}$ = 1 min, and recovery time, $T_{90–10\%}$ = 3 min) at a temperature close to 180 °C [133].

The selectivity toward various target gases such as sulfur dioxide (SO_2), ammonia (NH_3), hydrogen sulfide (H_2S), nitrogen dioxide (NO_2) has been discussed before. For instance, 95% sensing response of $CoFe_2O_4$ observes toward NO_2 compared to other gases at an operating temperature of 150°C, 5 seconds response time and 117 seconds recovery time with NO_2 gas [23]. Performing the same sensors for SO_2, NH_3, and H_2S was given just 3%, 6%, and 7%, respectively. The ferrites such as $NiFe_2O_4$, $ZnFe_2O_4$, $MgFe_2O_4$, $ZnAl_2O_4$, $CoAl_2O_4$, and $MgAl_2O_4$ shows the gas response 10–20% for H_2S and 1–10% for NH_3 gas at 300°C operating temperature.

The sensing response of $GaFeO_3$ toward ethanol vapor at 350°C demonstrates that the resistance declines rapidly in the alcohol atmosphere which exhibited n-type behavior. The response characteristics of the sensors below 350°C for 1 ppm of methanol, ethanol, and isopropanol do not show any significant output. This is due to low thermal energy of the molecules to react with the surface adsorbed oxygen species [105]. **Table 6** illustrates some typical experimental results of gas sensing properties of perovskite-based materials.

http://dx.doi.org/10.5772/62559

Perovskite	Sensing material	Sensing response (%)	Response time (Sec.)	Recovery time (Sec.)	Response temperature (°C)	Refs.
$LaCoO_3$	CO	95	423	377	250	[134]
$AlNbO_3$	Ethanol	99	24	100	250	[109]
$ZnSnO_3$	H_2	95	1	12	>375	[135]
$ZnWO_4$	H_2O	98	15	158	R.T	[90]
$NiFe_2O_4$	H_2S	75	60	300	150	[136]
$CoWO_4$	NH_3	90	3	1	Elevated	[118]
$SmFe_{1-x}Co_xO_3$	O_3	<80	–	600	R.T	[137]
$La_{1-x}Sr_xFeO_3$	CO_2	<80	660	300	380	[138]
$LaFeO_3$	C_4H_{10}	93	–	–	250	[139]
$CuFe_2O_4$	LPG	86	5	68	350	[11]
Zn_2SnO_4	NO_2	–	43	326	200	[79]

Table 6. Practical efficiencies of some important perovskites-based sensors.

6. Summary and recommendation for future research

The oxygen partial pressure dependence of the point defect concentration, and its conductivity, in perovskite semiconductors allows for their application in sensors. The resistance of the as-mentioned semiconductors can be affected by other gases, such as O_2, CO, NH_3, hydrocarbons, and ethanol, which create opportunities for developing new chemical sensors.

In addressing diversity and establishing the current chapter, it is necessary to develop the sensors technology by routine reliable synthesis of self-assembled materials including inorganic materials or inorganic–organic nanocomposites for real-life applications and also commercialization. The need of novel perovskites sensing materials with suitable compositions from all reported perovskites (summarized in **Tables 4** and **5**) as a filler/cover for sensing device for an especial chemical. The need of high-accuracy sensing device in everyday life especially for health care and also environmental concerns requires a systematic management and researches. For example, a suitable combination of perovskite materials can be identified out of 15 components for ethanol sensors. Moreover, suitable manufacturing technologies, free choice of device geometrical properties to attain the indispensable dimensional efficiencies, optimization of surface for the occurrence of conductance, ease of production flow, and investment expenses are immediately required. It seems that the accurate optimization of perovskite materials applicable in gas sensor is influenced by temperature and partial pressure of oxygen. Therefore, the performance of gas sensor depends on the exact height from the sea level.

Author details

Morteza Enhessari* and Ali Salehabadi

*Address all correspondence to: enhessari@gmail.com/enhessari@iau-naragh.ac.ir

Department of Chemistry, Naragh Branch, Islamic Azad University, Naragh, Iran

References

[1] Atkins P., Overton T., Rourke J., Weller M., Armstrong F., Inorganic Chemistry, Fifth Edition, Oxford University Press, USA, 2006.

[2] Qi T., Levchenko SV, Bennett JW, Grinberg I., Rappe AM, New Prospects for High Performance SONAR, Chemical Sensor, and Communication Device Materials, DoD High Performance Computing Modernization Program Users Group, IEEE (2010) 197–204.

[3] Shimizu Y., Uemura K., Matsuda H., Miura N., Yamazoe N., Bi-functional oxygen electrode using large surface area $La_{1-x}Ca_xCoO_3$ for rechargeable metal-air battery, J. Electrochem. Soc. 137 (1990) 3430–3433.

[4] Hunter GW, Xu JC, Evans LJ, Vander Wal RL, Gordon M., Chemical sensors based on metal oxide nanostructures, applications: Solid-state ionic devices, 9(2006)199–209.

[5] Shaterian M., Enhessari M., Rabbani D., Asghari M., Synthesis, characterization and photocatalytic activity of $LaMnO_3$ nanoparticles, Appl. Surf. Sci. 318 (2014) 213–217.

[6] Ghasdi M., Alamdari H., CO sensitive nanocrystalline $LaCoO_3$ perovskite sensor prepared by high energy ball milling, Sensors Actuators B Chem. 148 (2010) 478–485.

[7] Wang L., Kumar RV, Thick film miniaturized HCl gas sensor, Sensors Actuators B Chem. 98 (2004) 196–203.

[8] Pokhrel S., Huo L., Zhao H., Gao S., Thick film of $LaCr_{1-x}Ti_xO_3$ (x = 0.4) perovskites prepared by combustion technique for alcohol sensing application, Sensors Actuators B Chem. 122 (2007) 321–327.

[9] Luyten J., Chemical and electrical properties of Yb-doped strontium cerates in coal combustion atmospheres, Solid State Ion. 46 (1991) 117–120.

[10] Guoxi X., Yuebin X., Effects on magnetic properties of different metal ions substitution cobalt ferrites synthesis by sol–gel auto-combustion route using used batteries, Mater. Lett. 164 (2016) 444–448.

[11] Khandekar MS, Tarwal NL, Patil JY, Shaikh FI, Mulla IS, Suryavanshi SS, Liquefied petroleum gas sensing performance of cerium doped copper ferrite, Ceram. Int. 39 (2013) 5901–5907.

[12] Enhessari M., Khanahmadzadeh S., Ozaee K., Structural characterization of $BaZrO_3$ nanopowders prepared by stearic acid gel method, J. Iran. Chem. Res. 3 (2010) 11–15.

[13] Shandiz RH, Shaterian M., Ozaee K., Enhessari M., Fabrication of low temperature gas sensor using $SrCe_{0.9}Yb_{0.1}O_3$ nanopowders as proton conductor, Synth. React. Inorg. Met. Nano-Metal Chem. 45 (2013) 1108–1111.

[14] Shaterian M., Barati M., Ozaee K., Enhessari M., Application of $MnTiO_3$ nanoparticles as coating layer of high performance $TiO_2/MnTiO_3$ dye-sensitized solar cell, J. Ind. Eng. Chem. 20 (2013) 3646–3648.

[15] Enhessari M., Salehabadi A., Nasrollahi Z., Ozaee K., Ammonia-assisted synthesis method for $CoTiO_3$ nanoporous matrix, J. Semicond. 37 (2016) 1–3.

[16] Huang X., Choi Y., Chemical sensors based on nanostructured materials, Sensors and Actuators B, 122 (2006) 659–671.

[17] Mukherjee K., Majumder SB, Hydrogen sensing characteristics of nano-crystalline $Mg_{0.5}Zn_{0.5}Fe_2O_4$ thin film: Effect of film thickness and operating temperature, Int. J. Hydrogen Energy 39 (2014) 1185–1191.

[18] Chang CC, Tang CS, An integrated pyroelectric infrared sensor with a PZT thin film, Sensors Actuators A Phys. 65 (1998) 171–174.

[19] Shi C., Qin H., Zhao M., Wang X., Li L., Hu J., Investigation on electrical transport, CO sensing characteristics and mechanism for nanocrystalline $La_{1-x}Ca_xFeO_3$ sensors, Sensors Actuators B Chem. 190 (2014) 25–31.

[20] Andre RS, Zanetti SM, Varela JA, Longo E., Synthesis by a chemical method and characterization of $CaZrO_3$ powders: Potential application as humidity sensors, B2 Ceram. Int. 40 (2014) 16627–16634.

[21] Chow CL, Huang H., Ang WC, Liu H., Huang Y., Tse MS, et al., Effect of annealing temperature on the crystallization and oxygen sensing property of strontium titanate ferrite sol–gel thin films, Sensors Actuators B Chem. 187 (2013) 20–26.

[22] Roffat M., Noël O., Soppera O., Bohnke O., Investigation of the perovskite ceramic $Li_{0.30}La_{0.56}Ti\ O_3$ by Pulsed Force Mode AFM for p H sensor application, Sensors Actuators B Chem. 138 (2009) 193–200.

[23] Bagade AA., Rajpure KY, Development of $CoFe_2O_4$ thin films for nitrogen dioxide sensing at moderate operating temperature, J. Alloys Compd. 657 (2016) 414–421.

[24] Dharmadhikari DV, Nikam SK, Athawale AA, Template free hydrothermal synthesis and gas sensing application of lanthanum cuprate (La_2CuO_4): Effect of precursors on phase formation and morphology, J. Alloys Compd. 590 (2014) 486–493.

[25] Enhessari M., Razi MK, Etemad L., Parviz A., Sakhaei M., Structural, optical and magnetic properties of the Fe_2TiO_5 nanopowders, J. Exp. Nanosci. 9 (2014) 167–176.

[26] Sadjadi MS, Mozaffari M., Enhessari M., Zare K., Superlattices and microstructures effects of $NiTiO_3$ nanoparticles supported by mesoporous MCM-41 on photoreduction of methylene blue under UV and visible light irradiation, Superlattices Microstruct. 47 (2010) 685–694.

[27] Sadjadi M.S., Zare K., Khanahmadzadeh S., Enhessari M., Structural characterization of $NiTiO_3$ nanopowders prepared by stearic acid gel method, Mater. Lett. 62 (2008) 3679–3681.

[28] Enhessari M., Parviz A., Ozaee K., Karamali E., Magnetic properties and heat capacity of $CoTiO_3$ nanopowders prepared by stearic acid gel method, J. Exp. Nanosci. 5 (2010) 61–68.

[29] Enhessari M., Shaterian M., Esfahani MJ, Motaharian MN, Synthesis, characterization and optical band gap of La_2CuO_4 nanoparticles, Mater. Sci. Semicond. Process. 16 (2013) 1517–1520.

[30] Zare K., Sadjadi MS, Enhessari M., Khanahmadzadeh S., Synthesis and characterization of $PbTiO_3$ nanopowders by citric acid gel method, J. Phys. Theor. Chem. 6 (2009) 9–12.

[31] Ghasdi M., Alamdari H., Royer S., Adnot A., Electrical and CO gas sensing properties of nanostructured $La_{1-x}Ce_xCoO_3$ perovskite prepared by activated reactive synthesis, Sensors Actuators B Chem. 156 (2011) 147–155.

[32] Zhou L., Li X., Wu H., Liao Z., Yuan Q., Xia F., et al., Sensing properties of YSZ-based NOx sensors with double-perovskite $(La_{0.8}Sr_{0.2})_2FeNiO_6$-sensing electrodes, Ceram. Int. 40 (2014) 9257–9263.

[33] Mulmi S., Kannan R., Thangadurai V., CO_2 and SO_2 tolerant Fe-doped metal oxides for solid state gas sensors, Solid State Ion. 262 (2014) 274–278.

[34] Lancaster D., Weidner R., Richter D., Tittel F., Limpert J., Compact CH4 sensor based on difference frequency mixing of diode lasers in quasi-phasematched $LiNbO_3$, Opt. Commun. 175 (2000) 461–468.

[35] Fergus JW, Perovskite oxides for semiconductor-based gas sensors, Sensors Actuators B Chem. 123 (2007) 1169–1179.

[36] Wang X., Qin H., Sun L., Hu J., CO_2 sensing properties and mechanism of nanocrystalline $LaFeO_3$ sensor, Sensors Actuators B Chem. 188 (2013) 965–971.

[37] Patil LA, Suryawanshi DN, Pathan IG, Patil DG, Effect of firing temperature on gas sensing properties of nanocrystalline perovskite $BaTiO_3$ thin films prepared by spray pyrolysis techniques, Sensors Actuators B Chem. 195 (2014) 643–650.

[38] Giang HT, Duy HT, Ngan PQ, Thai GH, Thi D., Thu A., High sensitivity and selectivity of mixed potential sensor based on Pt/YSZ/$SmFeO_3$ to NO_2 gas, Sensors Actuators B Chem. 183 (2013) 550–555.

[39] Giang HT, Duy HT, Ngan PQ, Thai GH, Thi D., Thu A., et al., Hydrocarbon gas sensing of nano-crystalline perovskite oxides $LnFeO_3$ (Ln = La, Nd and Sm), Sensors Actuators B Chem. 158 (2011) 246–251.

[40] Dhivya P., Prasad AK, Sridharan M., Nanostructured perovskite $CdTiO_3$ films for methane sensing, Sensors Actuators B. Chem. 222 (2015) 987–993.

[41] Ishihara T., Perovskite Oxide for Solid Oxide Fuel Cells, Springer, New York, USA, 2009.

[42] Armstrong EN, Striker T., Ramaswamy V., Ruud JA, Wachsman ED, NO_x adsorption behavior of $LaFeO_3$ and $LaMnO_{3+\delta}$ and its influence on potentiometric sensor response, Sensors Actuators B Chem. 158 (2011) 159–170.

[43] Michael L., Brian W., Post ML, Sanders BW, Kennepohl P., Thin films of non-stoichiometric perovskites as potential oxygen sensors, Sensors Actuators B Chem. 1 (1993) 272–275.

[44] Post M., Tunney J., Yang D., Du X., Singleton D., Material chemistry of perovskite compounds as chemical sensors, Sensors Actuators B Chem. 59 (1999) 190–194.

[45] Sarker MRH, Karim H., Martinez R., Delfin D., Enriquez R., Shuvo MAI, Temperature measurements using a lithium niobate ($LiNbO_3$) pyroelectric ceramic, Measurement 75 (2015) 104–110.

[46] Tasaki T., Takase S., Shimizu Y., Impedance metric acetylene gas sensing properties of Sm–Fe-based perovskite-type oxide-based thick-film device, Sensors Actuators B Chem. 187 (2013) 128–134.

[47] Gupta R., YBCO-FET room temperature ammonia sensor, Sensors Actuators B Chem. 63 (2000) 35–41.

[48] Deng J., Zhu W., Tan OK, Yao X., Amorphous $Pb(Zr,Ti)O_3$ thin film hydrogen gas sensor, Sensors and Actuators B, 77 (2001) 416–420.

[49] Yannopoulos LN, A p-type semiconductor thick film gas sensor, Sensors Actuators 12 (1987) 263–273.

[50] Šutka A., Gross KA, Spinel ferrite oxide semiconductor gas sensors, Sensors Actuators B Chem. 222 (2016) 95–105.

[51] Choopun S., Wongrat E., N. Hongsith, Metal-oxide nanowires for gas sensors, Met-Oxide Nanowires Gas Sensors, 2012: pp. 3–24.

[52] Argirusis C., Jomard F., Wagner SF, Menesklou W., Ivers-Tiffée E., Study of the oxygen incorporation and diffusion in $Sr(Ti_{0.65}Fe_{0.35})O_3$ ceramics, Solid State Ion. 192 (2011) 9–11.

[53] Isarakorn D., Briand D., Sambri A., Gariglio S., Triscone JM, Guy F., et al., Finite element analysis and experiments on a silicon membrane actuated by an epitaxial PZT thin film for localized-mass sensing applications, Sensors Actuators B Chem. 153 (2011) 54–63.

[54] Wang L., He Y., Hu J., Qi Q., Zhang T., DC humidity sensing properties of $BaTiO_3$ nanofiber sensors with different electrode materials, Sensors Actuators B Chem. 153 (2011) 460–464.

[55] Imran Z., Batool SS, Jamil H., Usman M., Israr-Qadir M., Shah SH, et al., Excellent humidity sensing properties of cadmium titanate nanofibers, Ceram. Int. 39 (2013) 457–462.

[56] Zhang Y., Fu W., Yang H., Li M., Li Y., Zhao W., et al., A novel humidity sensor based on $Na_2Ti_3O_7$ nanowires with rapid response-recovery, Sensors Actuators B Chem. 135 (2008) 317–321.

[57] J. Yoon, G. Hunter, S. Akbar, Dutta PK, Interface reaction and its effect on the performance of a CO_2 gas sensor based on $Li_{0.35}La_{0.55}Ti\ O_3$ electrolyte and Li_2CO_3 sensing electrode, Sensors Actuators B Chem. 182 (2013) 95–103.

[58] Chapelle A., Yaacob MH, Pasquet I., Presmanes L., BarnabéA., Tailhades P., et al., Structural and gas-sensing properties of $CuO–Cu_xFe_{3–x}O_4$ nanostructured thin films, Sensors Actuators B Chem. 153 (2011) 117–124.

[59] Mukherjee K., Majumder SB, Synthesis of embedded and isolated $Mg_{0.5}Zn_{0.5}Fe_2O_4$ nanotubes and investigation on their anomalous gas sensing characteristics, Sensors Actuators B Chem. 177 (2013) 55–63.

[60] Meuffels P., Propane gas sensing with high-density $SrTi_{0.6}Fe_{0.4}O_{(3–\delta)}$ ceramics evaluated by thermogravimetric analysis, J. Eur. Ceram. Soc. 27 (2007) 285–290.

[61] Iio A., Ikeda H., Anggraini SA, Miura N., Potentiometric YSZ-based oxygen sensor using $BaFeO_3$ sensing-electrode, Electrochem. Commun. 48 (2014) 134–137.

[62] Cavalieri A., Caronna T., Natali Sora I., Tulliani JM, Electrical characterization of room temperature humidity sensors in $La_{0.8}Sr_{0.2}Fe_{1–x}Cu_xO_3$ (x =0, 0.05, 0.10), Ceram. Int. 38 (2012) 2865–2872.

[63] Casas-Cabanas M., Chadwick AV, Palacín MR, Michel CR, Carbon dioxide sensing properties of bismuth cobaltite, Sensors Actuators B Chem. 157 (2011) 380–387.

[64] Gómez L., Galeano V., Parra R., Michel C.R., Paucar C., Morán O., Carbon dioxide gas sensing properties of ordered oxygen deficient perovskite $LnBaCo_2O_{5+\delta}$ (Ln = La, Eu), Sensors Actuators B Chem. 221 (2015) 1455–1460.

[65] Malavasi L., Tealdi C., Flor G., Chiodelli G., Cervetto V., Montenero A., et al., $NdCoO_3$ perovskite as possible candidate for CO-sensors: Thin films synthesis and sensing properties, Sensors Actuators B Chem. 105 (2005) 407–411.

[66] Michel CR, Delgado E., Martínez AH, Evidence of improvement in gas sensing properties of nanostructured bismuth cobaltite prepared by solution-polymerization method, Sensors Actuators B Chem. 125 (2007) 389–395.

[67] Shuk P., Vecher A., Kharton V., Tichonova L., Wiemhöfer HD, Guth U., et al., Electrodes for oxygen sensors based on rate earth manganites or cabaltites, Sensors Actuators B Chem. 16 (1993) 401–405.

[68] Tealdi C., Islam MS, Fisher CAJ., Malavasi L., Flor G., Defect and transport properties of the $NdCoO_3$ catalyst and sensor material, Prog. Solid State Chem. 35 (2007) 491–499.

[69] Wei X., Wei T., Li J., Lan X., Xiao H., Lin YS, Strontium cobaltite coated optical sensors for high temperature carbon dioxide detection, Sensors Actuators B Chem. 144 (2010) 260–266.

[70] Mullen MR, Spirig JV, Hoy J., Routbort JL, Singh D., Dutta PK, Development of nanosized lanthanum strontium aluminum manganite as electrodes for potentiometric oxygen sensor, Sensors Actuators B Chem. 203 (2014) 670–676.

[71] Wei XT, Wei T., Xiao H., Lin YS, Terbium doped strontium cerate enabled long period fiber gratings for high temperature sensing of hydrogen, Sensors Actuators B Chem. 152 (2011) 214–219.

[72] Schutter FD, Vangrunderbeek J., Luyten J., Proton conductivity in strontium cerates for hydrogen gas sensors in coal gasification systems, Solid State Ionics. 57 (1992) 77–81.

[73] Zhou H., Dai L., Jia L., Zhu J., Li Y., Wang L., Effect of fluorine, chlorine and bromine doping on the properties of gadolinium doped barium cerate electrolytes, Int. J. Hydrogen Energy 40 (2015) 8980–8988.

[74] Zhang M., Hu C., Liu H., Xiong Y., Zhang Z., A rapid-response humidity sensor based on $BaNbO_3$ nanocrystals, Sensors Actuators B Chem. 136 (2009) 128–132.

[75] Gnanasekar KI, Jayaraman V., Prabhu E., Gnanasekaran T., Periaswami G., Electrical and sensor properties of $FeNbO_4$: A new sensor material, Sensors Actuators B Chem. 55 (1999) 170–174.

[76] Xuchen L., Preparation and characterization of $LaNiO_3$ A r F ratio-sensitive thin film by sol–gel process based on amorphous citrate precursors, (2000) 24–28.

[77] Kocemba I., Wróbel-Jedrzejewska M., Szychowska A., Rynkowski J., Główka M., The properties of barium stannate and aluminum oxide-based gas sensor. The role of Al_2O_3 in this system, Sensors Actuators B Chem. 121 (2007) 401–405.

[78] Song P., Wang Q., Yang Z., Ammonia gas sensor based on PPy/$ZnSnO_3$ nanocomposites, Mater. Lett. 65 (2011) 430–432.

[79] Ganbavle VV, Patil MA, Deshmukh HP, Rajpure KY, Development of $Zn_2Sn\ O_4$ thin films deposited by spray pyrolysis method and their utility for NO_2 gas sensors at moderate operating temperature, J. Anal. Appl. Pyrolysis 107 (2014) 233–241.

[80] Huang J., Xu X., Gu C., Wang W., Geng B., Sun Y., et al., Size-controlled synthesis of porous $ZnSnO_3$ cubes and their gas-sensing and photocatalysis properties, Sensors Actuators B Chem. 171–172 (2012) 572–579.

[81] Jiang YQ, Chen XX, Sun R., Xiong Z., Zheng LS, Hydrothermal syntheses and gas sensing properties of cubic and quasi-cubic $Zn_2Sn\ O_4$, Mater. Chem. Phys. 129 (2011) 53–61.

[82] Tharsika T., Haseeb ASMA, Akbar SA, Sabri MFM, Wong YH, Gas sensing properties of zinc stannate ($Zn_2Sn\ O_4$) nanowires prepared by carbon assisted thermal evaporation process, J. Alloys Compd. 618 (2015) 455–462.

[83] Upadhyay S., Kavitha P., Lanthanum doped barium stannate for humidity sensor, Mater. Lett. 61 (2007) 1912–1915.

[84] Zhou M., Ahmad A., Sol–gel processing of In-doped $CaZrO_3$ solid electrolyte and the impedimetric sensing characteristics of humidity and hydrogen, Sensors Actuators B Chem. 129 (2008) 285–291.

[85] Saha D., Giri R., Mistry KK, Sengupta K., Magnesium chromate-TiO_2 spinel tape cast thick film as humidity sensor, Sensors Actuators B Chem. 107 (2005) 323–331.

[86] Pingale S., Patil S., Vinod M., Pathak G., Vijayamohanan K., Mechanism of humidity sensing of Ti-doped $MgCrO_3$ ceramics, Materials Chemistry and Physics. 46 (1996) 72–76.

[87] Sears WM, The gas-sensing properties of sintered bismuth iron molybdate catalyst, Sensors Actuators 19 (1989) 351–370.

[88] Edwin Suresh Raj AM, Mallika C., Swaminathan K., Sreedharan OM, Nagaraja KS, Zinc(II) oxide-zinc(II) molybdate composite humidity sensor, Sensors Actuators B Chem. 81 (2002) 229–236.

[89] Sundaram R., Nagaraja KS, Solid state electrical conductivity and humidity sensing studies on metal molybdate–molybdenum trioxide composites (M = Ni^{2+}, Cu^{2+} and Pb^{2+}), Sensors Actuators B Chem. 101 (2004) 353–360.

[90] You L., Cao Y., Sun YF, Sun P., Zhang T., Du Y., et al., Humidity sensing properties of nanocrystalline $ZnWO_4$ with porous structures, Sensors Actuators B Chem. 161 (2012) 799–804.

[91] Gonzalez CM, Du X., Dunford JL, Post ML, Copper tungstate thin-films for nitric oxide sensing, Sensors Actuators B Chem. 173 (2012) 169–176.

[92] Tamaki J., Fujii T., Fujimori K., Miura N., Yamazoe N., Application of metal tungstate-carbonate composite to nitrogen oxides sensor operative at elevated temperature, Sensors Actuators B Chem. 25 (1995) 396–399.

[93] Solis V., Lantto JL, A study of gas-sensing properties of sputtered films, Sensors Actuators B 25 (1995) 591–595.

[94] Solis JL, Lantto V., Haggstrom L., Kalska B., Frantti J., Saukko S., Synthesis of new compound semiconductors in the Sn–W–O system for gas-sensing studies, Sensors Actuators B 68 (2000) 286–292.

[95] Kärkkänen I., Kodu M., Avarmaa T., Kozlova J., Matisen L., Mändar H., et al., Sensitivity of $CoWO_4$ thin films to CO, Procedia Eng. 5 (2010) 160–163.

[96] Suresh Raj AME, Mallika C., Sreedharan O., Nagaraja K., Manganese oxide–manganese tungstate composite humidity sensors, Mater. Lett. 53 (2002) 316–320.

[97] Yadav BC, Yadav A., Singh S., Singh K., Nanocrystalline zinc titanate synthesized via physicochemical route and its application as liquefied petroleum gas sensor, Sensors Actuators B Chem. 177 (2013) 605–611.

[98] Santhaveesuk T., Gardchareon A., Wongratanaphisan D., Choopun S., Ethanol sensing properties of $Zn_2Ti\ O_4$ particles, Ceram. Int. 41 (2015) S809–S813.

[99] Du J., Wu Y., Choy K-L, Shipway PH, Structure, properties and gas sensing behavior of $Cr_{2-x}Ti_xO_3$ films fabricated by electrostatic spray assisted vapour deposition, Thin Solid Films 519 (2010) 1293–1299.

[100] Belle CJ, Wesch GE, Neumeier S., Lozano-Rodríguez MJ, Scheinost AC, Simon U., Volume-doped cobalt titanates for ethanol sensing: An impedance and X-ray absorption spectroscopy study, Sensors Actuators B Chem. 192 (2014) 60–69.

[101] Sutka A., Mezinskis G., Lusis A., Stingaciu M., Gas sensing properties of Zn-doped p-type nickel ferrite, Sensors Actuators B Chem. 171–172 (2012) 354–360.

[102] Franke D., Zosel J., Guth U., NO sensitivity of perovskite-type electrode materials $La_{0.6}Ca_{0.4}B'_{1-x}B''_xO_{3\pm\delta}$ (B′ = Mn, Cr; B″ = Ni, Fe, Co; x = 0, 0.1, …, 0.6) in mixed potential sensors, Sensors Actuators B Chem. 223 (2016) 723–729.

[103] Lee I., Jung B., Park J., Lee C., Hwang J., Park CO, Mixed potential NH_3 sensor with $LaCoO_3$ reference electrode, Sensors Actuators B Chem. 176 (2013) 966–970.

[104] Khandekar MS, Tarwal NL, Mulla IS, Suryavanshi SS, Nanocrystalline Ce doped $CoFe_2O_4$ as an acetone gas sensor, Ceram. Int. 40 (2014) 447–452.

[105] Sen S., Chakraborty N., Rana P., Narjinary M., Mursalin SD, Tripathy S., et al., Nanocrystalline gallium ferrite: A novel material for sensing very low concentration of alcohol vapour, Ceram. Int. 41 (2015) 10110–10115.

[106] Kazin AP, Rumyantseva MN, Prusakov VE, Suzdalev IP, Gaskov AM, Nanocrystalline ferrites $Ni_xZn_{1-x}Fe_2O_4$: Influence of cation distribution on acidic and gas sensing properties, J. Solid State Chem. 184 (2011) 2799–2805.

[107] Balamurugan C., Vijayakumar E., Subramania A., Synthesis and characterization of In Nb O_4 nanopowder for gas sensors, Talanta 88 (2012) 115–20.

[108] Zhu Q., Shih W-H, Shih WY, Enhanced dimethyl methylphosphonate (DMMP) detection sensitivity by lead magnesium niobate-lead titanate/copper piezoelectric microcantilever sensors via Young's modulus change, Sensors Actuators B Chem. 182 (2013) 147–155.

[109] Balamurugan C., Subashini A., Chaudhari GN, Subramania A., Development of wide band gap sensor based on $AlNbO_4$ nanopowder for ethanol, J. Alloys Compd. 526 (2012) 110–115.

[110] Zhang D., Zhang R., Xu C., Fan Y., Yuan B., Microwave-assisted solvothermal synthesis of nickel molybdate nanosheets as a potential catalytic platform for NADH and ethanol sensing, Sensors Actuators B Chem. 206 (2015) 1–7.

[111] Raju AR, Rae CNR, MoO_3/TiO_2 and Bi_2MoO_6 as ammonia sensors, Sensors Actuators B Chem. 21 (1994) 23–26.

[112] Sivapunniyam A., Wiromrat N., Myint MTZ, Dutta J., High-performance liquefied petroleum gas sensing based on nanostructures of zinc oxide and zinc stannate, Sensors Actuators B Chem. 157 (2011) 232–239.

[113] Farahani H., Wagiran R., Hamidon MN, Humidity sensors principle, mechanism, and fabrication technologies: A comprehensive review, Sensors (2014) 7881–7939.

[114] Zhou ZG, Tang ZL, Zhang ZT, Wlodarski W., Perovskite oxide of PTCR ceramics as chemical sensors, Sensors Actuators B Chem. 77 (2001) 22–26.

[115] Balamurugan C., Bhuvanalogini G., Subramania A., Development of nanocrystalline $CrNbO_4$ based p-type semiconducting gas sensor for LPG, ethanol and ammonia, Sensors Actuators B Chem. 168 (2012) 165–171.

[116] Feng C., Ruan S., Li J., Zou B., Luo J., Chen W., et al., Ethanol sensing properties of $LaCo_xFe_{1-x}O_3$ nanoparticles: Effects of calcination temperature, Co-doping, and carbon nanotube-treatment, Sensors Actuators B. Chem. 155 (1991) 232–238.

[117] Huck C., Poghossian A., Bäcker M., Chaudhuri S., Zander W., Schubert J., et al., Capacitively coupled electrolyte-conductivity sensor based on high-k material of barium strontium titanate, Sensors Actuators B Chem. 198 (2014) 102–109.

[118] Diao Q., Yang F., Yin C., Li J., Yang S., Liang X., et al., Ammonia sensors based on stabilized zirconia and $CoWO_4$ sensing electrode, Solid State Ion. 225 (2012) 328–331.

[119] StankevičV., ŠimkevičiusČ., Keršulis S., Balevičius S., ŽurauskienėN., Pavilonis D., et al., Improvement in the long-term stability of parameters of encapsulated magnetic

field sensors based on LaSrMnO thin films, Sensors Actuators A Phys. 228 (2015) 112–117.

[120] Wang Y., Xu Y., Luo L., Ding Y., Liu X., Huang A., A novel sensitive nonenzymatic glucose sensor based on perovskite $LaNi_{0.5}Ti_{0.5}O_3$-modified carbon paste electrode, Sensors Actuators B Chem. 151 (2010) 65–70.

[121] Shahnavaz Z., Lorestani F., Alias Y., Woi PM, Polypyrrole–$ZnFe_2O_4$ magnetic nanocomposite with core–shell structure for glucose sensing, Appl. Surf. Sci. 317 (2014) 622–629.

[122] Nossov A., Rinkevich A., Rigmant M., Vassiliev V., Combined lanthanum manganite magnetoresistive-fluxgate magnetic field sensor, Sensors Actuators A Phys. 94 (2001) 157–160.

[123] Xu Y., Memmert U., Hartmann U., Magnetic field sensors from polycrystalline manganites, Sensors Actuators A 91 (2001) 26–29.

[124] Rubi D., Fontcuberta J., Lacaba M., González AM, Baztán J., Calleja A., On–off magnetoresistive sensor based on screen-printed $La_{2/3}Sr_{1/3}Mn\ O_3$ manganite, Sensors Actuators A Phys. 132 (2006) 52–55.

[125] Balcells L., Calvo E., Fontcuberta J., Room-temperature anisotropic magnetoresistive sensor based on manganese perovskite thick films, J. Magn. Magn. Mater. 242–245 (2002) 1166–1168.

[126] Jung H.-R., Lee S.-G., Kim M.-H., Yeo J.-H., Structural and electrical properties of $Ni_xMn_{3-x}O_4$ system ceramics for infrared sensors, Microelectron. Eng. 146 (2015) 109–112.

[127] Shinagawa M., Kobayashi J., Yagi S., Sakai Y., Sensitive electro-optic sensor using $KTa_{1-x}Nb_xO_3$ crystal, Sensors Actuators A Phys. 192 (2013) 42–48.

[128] Sun LL, Tan OK, Liu WG, Zhu WG, Yao X., Poling of multilayer $Pb(Zr_{0.3}Ti_{0.7})O_3$/$PbTiO_3$ thin film for pyroelectric infrared sensor application, Infrared Phys. Technol. 44 (2003) 177–182.

[129] Shahnavaz Z., Woi PM., Alias Y., A hydrothermally prepared reduced graphene oxide-supported copper ferrite hybrid for glucose sensing, Ceram. Int. 41 (2015) 12710–12716.

[130] Fine GF, Cavanagh LM, Afonja A., Binions R., Metal oxide semi-conductor gas sensors in environmental monitoring, Sensors 10 (2010) 5469–5502.

[131] Filipovic L., Selberherr S., Performance and stress analysis of metal oxide films for CMOS-integrated gas sensors, Sensors 15 (2015) 7206–7227.

[132] Wang Y., Liu B., Xiao S., Li H., Wang L., Cai D., High performance and negative temperature coefficient of low temperature hydrogen gas sensors using palladium decorated tungsten oxide, J. Mater. Chem. A 3 (2014) 1317–1324.

[133] Addabbo T., Bertocci F., Fort A., Mugnaini M., Shahin L., Vignoli V., An artificial olfactory system (AOS) for detection of highly toxic gases in air based on $YCoO_3$, Procedia Eng. 87 (2014) 1095–1098.

[134] Ding J-C, Li H-Y, Cai Z-X, Wang X-X, Guo X., Near room temperature CO sensing by mesoporous $LaCoO_3$ nanowires functionalized with Pd nanodots, Sensors Actuators B Chem. 222 (2016) 517–524.

[135] Wadkar P., Bauskar D., Patil P., High performance H_2 sensor based on $ZnSnO_3$ cubic crystallites synthesized by a hydrothermal method, Talanta 105 (2013) 327–332.

[136] Ghosh P., Mukherjee A., Fu M., Chattopadhyay S., Mitra P., Influence of particle size on H_2 and H_2S sensing characteristics of nanocrystalline nickel ferrite, Phys. E Low-Dimensional Syst. Nanostructures 74 (2015) 570–575.

[137] Itagaki Y., Mori M., Hosoya Y., Aono H., Sadaoka Y., O_3 and NO_2 sensing properties of Sm $Fe_{1-x}Co_xO_3$ perovskite oxides, Sensors Actuators B Chem. 122 (2007) 315–320.

[138] Fan K., Qin H., Wang L., Ju L., Hu J., CO_2 gas sensors based on $La_{1-x}Sr_xFeO_3$ nanocrystalline powders, Sensors Actuators B Chem. 177 (2013) 265–269.

[139] Bhargav KK, Maity A., Ram S., Majumder SB, Low temperature butane sensing using catalytic nano-crystalline lanthanum ferrite sensing element, Sensors Actuators B Chem. 195 (2014) 303–312.

[140] Verma N., Singh S., Srivastava R., Yadav BC, Fabrication of iron titanium oxide thin film and its application as opto-electronic humidity and liquefied petroleum gas sensors, Opt. Laser Technol. 57 (2014) 181–188.

[141] Addabbo T., Bertocci F., Fort A., Gregorkiewitz M., Mugnaini M., Spinicci R., et al., Gas sensing properties and modeling of $YCoO_3$ based perovskite materials, Sensors Actuators B Chem. 221 (2015) 1137–1155.

[142] Ding J-C, Li H-Y, Guo X., CO sensing mechanism of $LaCoO_3$, Solid State Ionics. 272 (2015) 155–159.

[143] Sutka A., Mezinskis G., Lusis A., Jakovlevs D., Influence of iron non-stoichiometry on spinel zinc ferrite gas sensing properties, Sensors Actuators B Chem. 171–172 (2012) 204–209.

[144] Karthick Kannan P., Saraswathi R., Impedimetric detection of alcohol vapours using nanostructured zinc ferrite, Talanta 129 (2014) 545–551.

[145] Zhao L., Steinhart M., Yosef M., Lee SK, Schlecht S., Large-scale template-assisted growth of $LiNbO_3$ one-dimensional nanostructures for nano-sensors, Sensors Actuators B Chem. 109 (2005) 86–90.

[146] Cheng H., Lu ZG, Synthesis and gas-sensing properties of $CaSnO_3$ microcubes, Solid State Sci. 10 (2008) 1042–1048.

[147] Machappa T., Badrunnisa S., Ambika Prasad MVN, Zinc tungstate ($ZnWO_4$) doped polyaniline (PANI) as humidity and gas sensing composite, Sens. Bio-Sensing Res. (2015).

[148] Singh J., Srivastava M., Kalita P., Malhotra B.D., A novel ternary Ni Fe_2O_4/Cu O/Fe O-chitosan nanocomposite as a cholesterol biosensor, Process Biochem. 47 (2012) 2189–2198.

[149] Ensafi AA, Alinajafi HA, Jafari-Asl M., Rezaei B., Ghazaei F., Cobalt ferrite nanoparticles decorated on exfoliated graphene oxide, application for amperometric determination of NADH and H_2O_2, Mater. Sci. Eng. C 60 (2016) 276–284.

IntechOpen